

Many-body effects in x-ray absorption and magnetic circular dichroism spectra within the LSDA+DMFT framework

O. Šipr,^{1,*} J. Minár,² A. Scherz,³ H. Wende,⁴ and H. Ebert^{2,†}

¹*Institute of Physics of the AS CR v. v. i., Cukrovarnická 10, CZ-162 53 Prague, Czech Republic*

²*Universität München, Department Chemie, Butenandtstr. 5-13 E, D-81377 München, Germany*

³*Stanford Institute for Material and Energy Science, SLAC National Accelerator Laboratory, Menlo Park, California, USA*

⁴*Universität Duisburg-Essen, Fakultät für Physik and Center for Nanointegration Duisburg-Essen (CeNIDE), Lotharstr. 1, DE-47048 Duisburg, Germany*

(Received 17 May 2011; revised manuscript received 5 August 2011; published 8 September 2011)

The theoretical description of photoemission spectra of transition metals was greatly improved recently by accounting for the correlations between the d electrons within the local spin-density approximation (LSDA) plus dynamical mean-field theory (DMFT). We assess the improvement of the LSDA+DMFT over the plain LSDA in x-ray absorption spectroscopy, which—unlike the photoemission spectroscopy—is probing unoccupied electronic states. By investigating the $L_{2,3}$ edge x-ray absorption near-edge structure (XANES) and x-ray magnetic circular dichroism (XMCD) of Fe, Co, and Ni, we find that the LSDA+DMFT improves the LSDA results, in particular concerning the asymmetry of the L_3 white line. Differences with respect to the experiment, nevertheless, remain—particularly concerning the ratio of the intensities of the L_3 and L_2 peaks. The changes in the XMCD peak intensities invoked by the use of the LSDA+DMFT are a consequence of the improved description of the orbital polarization and are consistent with the XMCD sum rules. Accounting for the core hole within the final-state approximation does not generally improve the results. This indicates that to get more accurate $L_{2,3}$ edge XANES and XMCD spectra, one has to treat the core hole beyond the final-state approximation.

DOI: [10.1103/PhysRevB.84.115102](https://doi.org/10.1103/PhysRevB.84.115102)

PACS number(s): 78.70.Dm, 75.10.Lp, 71.15.Mb

I. INTRODUCTION

X-ray absorption spectroscopy (XAS) evolved into a powerful technique for studying the electronic as well as the geometric structure of solids. Its main strength includes chemical selectivity, angular-momentum selectivity, and ability to provide detectable signals even for low amounts of material. This makes it well suited for studying defects, adsorbates, or nanostructures. For studying magnetism, x-ray magnetic circular dichroism (XMCD) spectroscopy, based on exploring the energy dependence of the difference in the absorption of left- and right-circularly polarized x-rays in a magnetized sample, proved to be a very powerful tool.¹

An efficient use of x-ray absorption spectroscopy requires a significant input from theory. *Ab initio* calculations of x-ray absorption near-edge structure (XANES) and XMCD are usually quite successful in reproducing the positions of spectral peaks, fairly successful in reproducing their intensities, and less successful in reproducing detailed shapes of the peaks. The severity of the failures of the theory varies depending on what material is studied, which absorption edges are involved, and what purpose the spectroscopic measurement serves.

Magnetic $3d$ elements are often used in man-made materials with properties that are interesting both fundamentally and for their possible technological application. XAS at the $L_{2,3}$ edges of Fe, Co, and Ni is used to get information about electronic states of the d character, which dominate close to the Fermi energy E_F . *Ab initio* calculations based on the local spin-density approximation (LSDA) to the density-functional theory suffer here from some common deficiencies. One such deficiency is the inability to reproduce correctly the ratio of the intensities of the L_3 and L_2 white lines in the XANES. This has been ascribed to the lack of proper dynamic treatment

of the core hole.^{2,3} Other common deficiencies of *ab initio* calculations include lack of asymmetry of the theoretical XANES white line and underestimated the ratio of the L_3 and L_2 XMCD peak intensities.^{1,4,5} Having an *ab initio* method able to deliver a more accurate quantitative agreement with experiment would be a great help when dealing with complex systems. The procedurally simple XMCD sum rules^{6,7} proved to be very powerful in interpreting experiments but their use has limitations. A more robust way is to compare measured spectra to spectra of a well-defined reference material. The properties of the reference material may, nevertheless, differ from the properties of the investigated system and, moreover, a suitable reference may not be available. In such situations, a comparison with accurate and reliable calculations may be very useful.^{8–10}

Even though the $3d$ elemental transition metals (TMs) can be seen as moderately correlated materials, there are known effects where including correlations is necessary; e.g., the orbital magnetic moment μ_{orb} is underestimated by the LSDA, and the improved results can be obtained by accounting for the enhancement of the orbital polarization either via the scheme of Brooks (OP Brooks)¹¹ or via the LSDA+ U scheme.^{12,13} These schemes, however, account only for static effects of the electron self-energy. To describe the spectra, dynamical effects should be included as well. This can be achieved via the LSDA plus dynamical mean-field theory (DMFT) scheme. The LSDA+DMFT formalism proved to be rather successful when dealing with the photoemission spectra of $3d$ transition metals.^{14–17} One can, therefore, expect that this formalism might lead to a substantial improvement also for XANES and XMCD spectra. In particular, as the LSDA+DMFT method provides correct values for μ_{orb} ,^{18,19} one can presuppose that it should also lead to a better ratio of the L_3 and L_2 XMCD peak

intensities because these are, within certain considerations, related to μ_{orb} .⁶

Several approaches to calculate XAS beyond the effective single-particle model were employed in the past. Their main emphasis was, however, on the interaction between the core hole and the photoelectron. Early calculations were done within the crystal field and charge transfer multiplet formalism, which is essentially an atomic-like approach with the long-range order (band-structure) effects entering only in a perturbative way via fitted parameters.²⁰ This approach could be extended to *ab initio* molecular-orbital calculations for small clusters by reducing the computational costs via splitting the orbitals into those that are treated via the configuration interaction and those that are treated within the density-functional theory.²¹ The multichannel scattering formalism²² makes it possible to include also the influence of more distant neighbors while retaining a large deal of the configuration interaction treatment of the correlations between the photoelectron and the core hole (albeit using a free parameter, which characterizes the partial core-hole screening); however, the correlations between the *d* electrons were included via an *ad hoc* energy shift.²³ Another approach to include the interaction between the core hole and the photoelectron while accounting also for the long-range order is to solve the Bethe-Salpeter equation.^{24,25} This approach is quite powerful but also computationally very demanding and cannot be straightforwardly extended to systems with correlated *d* electrons.

Our focus is on describing the x-ray absorption spectra by using as good ground state as possible, i.e., including the long-range band-structure effects and the correlations in the valence and conduction bands. For this purpose, the LSDA+DMFT formalism seems to be convenient as it accounts both for the band-structure effects and for the dynamic correlations between the semilocalized *d* electrons. We focus on the $L_{2,3}$ edge spectra of Fe, Co, and Ni. We demonstrate that if the valence-band and conduction-band correlations are included, the calculated spectra improve with respect to the LSDA. However, the improvement still does not lead to a fully satisfying reproduction of the experimental data—not even if the core hole is included via the final-state approximation. Based on these results, we conclude that dealing with the dynamical aspects of the correlations between the core hole and the valence and conduction electrons is needed for further progress.

II. COMPUTATIONAL SCHEME

A detailed description of the implementation of the LSDA+DMFT within the Korringa-Kohn-Rostoker (KKR) band structure scheme can be found in previous publications.^{26,27} We summarize here just the major features. The LSDA+DMFT method belongs to Hubbard-*U* band-structure schemes, i.e., the one-electron LSDA Hamiltonian is extended by an additional Hubbard-Hamiltonian term, which explicitly describes the on-site interaction between (in our case) the *d* electrons. The many-body Hamiltonian is specified by parameters representing the Coulomb matrix elements.

The main idea of the DMFT is to map the periodic many-body problem onto an effective single-impurity problem

that has to be solved self-consistently. For this purpose, one describes the electronic properties of the system in terms of the single-particle Green's function $\hat{G}(E)$, which is determined by

$$[E - \hat{H}_{\text{LSDA}} - \hat{\Sigma}(E)]\hat{G} = \hat{1}, \quad (1)$$

where E is the complex energy, \hat{H}_{LSDA} is the LSDA Hamiltonian, and $\hat{\Sigma}$ is a single-site effective self-energy operator. Within the DMFT, the self-energy $\hat{\Sigma}(E)$ is a solution of the many-body problem of an impurity placed in an effective medium. This medium is described by the so-called bath Green's function \hat{G} connected to the Green's function $\hat{G}(E)$ by

$$\hat{G}^{-1}(E) = \hat{G}^{-1}(E) + \hat{\Sigma}(E). \quad (2)$$

For a more detailed description of the DMFT equations, the authors redirect the reader to one of the excellent reviews.^{28,29}

The self-energy $\hat{\Sigma}(E)$ and the bath Green's function $\hat{G}(E)$ have to be determined self-consistently. Technically, this is done in two steps. The first step is solving Eq. (1) by the means of spin-polarized fully relativistic KKR band structure method.³⁰ The integration over the \mathbf{k} points was done on a regular mesh, using 2600 points in the irreducible part of the Brillouin zone in the case of bcc Fe and fcc Ni and 900 points in the case of hcp Co. We used an angular momentum cutoff $\ell_{\text{max}} = 3$. The Vosko, Wilk, and Nusair parametrization for the local exchange and correlation potential was used.³¹ Our implementation of the LSDA+DMFT within the KKR method is consistent with the full-potential scheme. However, for closely packed metals such as Fe, Co, or Ni, the atomic sphere approximation (ASA) to the potential is quite accurate.^{32,33} Therefore, we relied on the ASA for our calculations. We verified on selected cases that the results obtained for the ASA and for the full potential are very similar and that the conclusions are the same.

In the second step of the LSDA+DMFT calculation, the self-energy $\hat{\Sigma}(E)$ has to be found according to Eq. (2). This is done by solving the many-body effective impurity problem, often referred to as the DMFT solver.^{28,29} We used perturbative solvers, either the spin-polarized *T*-matrix + FLEX solver³⁴ or the spin-polarized *T*-matrix approximation solver (TMA).³⁵ The use of perturbative solvers is justified in this LSDA+DMFT study because the correlation effects in pure *3d* TMs are not very pronounced. The results are very similar for both solvers. Unless explicitly stated otherwise, data for the TMA solver are shown here. For the intra-atomic Hund exchange interaction J , we take a common value of $J = 0.9$ eV.^{29,36} The screened on-site Coulomb interaction U is set to 1.7 eV for Fe, 2.3 eV for Co, and 2.8 eV for Ni. These values were chosen because they lead to good values of μ_{spin} and μ_{orb} (see Chadov *et al.*¹⁸ for an extensive study) and also to a correct description of angular resolved photoemission spectra.^{15–17} Similar values of U and J were used also by other authors dealing with these systems,^{37–39} even though it should be noted that the parameters U and J are not directly transferable from one work to another because they depend, among others, on the choice of the basis set.²⁹ Importantly, our results do not depend crucially on the choice of U —similar XAS and XMCD spectra were obtained if U was decreased or increased by about 0.5 eV. Our conclusions are thus general.

Our implementation of the LSDA+DMFT method is self-consistent not only in the self-energy $\hat{\Sigma}(E)$ but also in the charge density $\rho(\mathbf{r})$, i.e., in each iteration, a new potential is used to generate a new single-particle Green's function $\hat{G}(E)$ entering Eq. (2). During the self-consistency cycle, the self-energy $\hat{\Sigma}(E)$ is calculated either on a set of Matsubara frequencies (FLEX solver) or on the real energy axis (TMA solver). The x-ray absorption spectra are calculated as it is standard in the Green's function formalism, i.e., via the scattering-path operator obtained from the Green's function $\hat{G}(E)$.³⁰ The self-energy on the real axis above E_F , which is needed for evaluating the Green's function $\hat{G}(E)$ according to Eq. (1), is obtained via the Padé analytic continuation.⁴⁰

The LSDA accounts already to some extent for the correlation of the d electrons, so a corresponding term has to be subtracted, to avoid counting this interaction twice. As the LSDA is not formulated in a diagrammatic language, the definition of this “double counting term” is not unique. Various approaches are possible and several recipes exist in literature.^{41,42} One way to determine the double counting correction is to make *a priori* assumptions about the occupation of the correlated orbitals. In the limit of a uniform occupancy of these orbitals, the energy correction to the LSDA is due to “fluctuations” away from the spin-dependent orbitally averaged occupation. The interaction term in this around mean-field (AMF) limit is⁴³

$$V_{m\sigma}^{\text{LSDA+AMF}} = \sum_{m'} U_{mm'} (n_{m'-\sigma} - n_{-\sigma}^0) + \sum_{m' \neq m} (U_{mm'} - J_{mm'}) (n_{m'\sigma} - n_{\sigma}^0). \quad (3)$$

In the above equation, $n_{m\sigma}$ is the occupation number for electrons with orbital and spin quantum numbers m and σ , n_{σ}^0 is the orbitally averaged occupation number, and $U_{mm'}$ and $J_{mm'}$ are matrix elements defined by the parameters U and J . The opposite limiting case concerning the occupation of the orbitals is the around atomic limit (AAL), which produces the correct behavior if $n_{m\sigma} = 0$ or 1. It is sometimes referred to as the fully localized limit (FLL) and the corresponding interaction term is⁴³

$$V_{m\sigma}^{\text{LSDA+AAL}} = V_{m\sigma}^{\text{LSDA+AMF}} - (U - J)(n_{\sigma}^0 - \frac{1}{2}). \quad (4)$$

The results of the LSDA+ U or LSDA+DMFT calculations may strongly depend on the choice of the double counting (d.c.) procedure. In this work, we are dealing with metals where the d electrons are not fully localized and their interaction is not very strong, so the uniform occupancy of the d orbitals is more realistic than the atomic limit. Consequently, we use the AMF d.c. correction. This is also in accordance with earlier experience with $3d$ TMs, especially in the field of photoemission.^{16,17} It is interesting to see whether this recipe works also for x-ray absorption spectroscopy (XAS).

We investigate also the effect of the core hole treated within the final-state approximation as fully relaxed and screened, i.e., with the potential calculated with one electron transferred from the $2p$ core level into the valence band. This was achieved by first performing a self-consistent calculation without the core hole and then by treating the photoabsorbing atom with the core hole as a perturbation, employing the impurity cluster Green's function method.⁴⁴⁻⁴⁶ In this impurity calculation,

the electronic structure was allowed to relax within the first two nearest-neighbor atomic shells around the photoabsorbing atom.

The theoretical spectra were broadened to account for the finite lifetimes of the core hole and of the photoelectron. The core hole related broadening was simulated by a Lorentzian with full width at half maximum of 0.40 eV at the L_3 edge and 0.70 eV at the L_2 edge, which is in the range of generally accepted values.^{47,48} The excited photoelectron related broadening was simulated by a Lorentzian with energy-dependent width, according to the “universal curve” as suggested by Müller *et al.*⁴⁹ A better agreement with experiment could be obtained if one assumed that the photoelectron damping starts at an onset energy E_s with an initial width A_s and increases further according to the universal curve, with E_s and A_s treated as free parameters.⁵⁰ However, this would have no influence on the conclusions.

Intuitive understanding as well as quantitative analysis of XMCD spectra has been greatly helped by the XMCD sum rules. These rules associate areas of XANES and XMCD peaks with μ_{spin} and μ_{orb} of the photoabsorbing atom. Our calculations provide μ_{spin} and μ_{orb} as well as XANES and XMCD spectra. Accordingly, application of the sum rules to our calculated spectra makes it possible to assess to what extent the changes in the spectra caused by including the valence- and conduction-band correlations via the LSDA+DMFT are consistent with the corresponding changes in the magnetic moments.

For the $L_{2,3}$ edge spectra, the sum rules can be written as^{6,7,51}

$$\frac{3}{I} \int (\Delta\mu_{L_3} - 2\Delta\mu_{L_2}) dE = \frac{\mu_{\text{spin}}^{(d)} + 7T_z^{(d)}}{n_h^{(d)}} \quad (5)$$

and

$$\frac{2}{I} \int (\Delta\mu_{L_3} + \Delta\mu_{L_2}) dE = \frac{\mu_{\text{orb}}^{(d)}}{n_h^{(d)}}, \quad (6)$$

where $\Delta\mu_{L_{2,3}}$ are the differences $\Delta\mu = \mu^{(+)} - \mu^{(-)}$ between the absorption coefficients for the left and right circularly polarized light at the L_2 and L_3 edges, I is the integrated isotropic absorption spectrum, $\mu_{\text{spin}}^{(d)}$ and $\mu_{\text{orb}}^{(d)}$ are the d components of the local spin and orbital magnetic moments, $n_h^{(d)}$ is the number of holes in the d band, and $T_z^{(d)}$ is the d component of the intra-atomic magnetic dipole operator for spin quantization axis aligned along z . The $T_z^{(d)}$ term is negligible for high-symmetry systems such as those dealt with here. However, this does not necessarily apply to more complex systems.⁵² Application of the sum rules (5)–(6) requires setting the energy cutoff E_C , which defines the upper boundary of the $3d$ band. We determined it by requiring that the integrated density of the d states is ten when integrated from the bottom of the valence band up to E_C , similar as in our earlier study.⁵²

III. EXPERIMENT

The bulklike Fe, Co, and Ni films were grown *in situ* directly at the synchrotron radiation facility BESSY II (Berlin, Germany). As a substrate, a Cu(100) single crystal was

used and the films were prepared at room temperature in ultrahigh vacuum conditions (base pressure 2×10^{-10} mbar) by evaporation from high-purity rods using a commercial triple e^- -beam evaporator. The surface of the Cu crystal was cleaned by several cycles of Ar^+ bombardment and annealing at $T = 900$ K. The deposition rates were in the regime of 1 \AA per minute. The Cu(100) single crystal and the films were characterized by means of low-energy electron diffraction (LEED) and Auger-electron spectroscopy (AES). The thickness of the ferromagnetic films was calibrated by AES and by the signal-to-background ratio (edge jump) at the respective $L_{2,3}$ edges. The thickness of the Fe film was 50 monolayers (ML) and 20 ML for the Co and Ni films. The experimental data have been obtained accounting for saturation effects, and the XMCD spectra have been corrected to correspond to 100% circular polarization and collinear orientation of the photon \mathbf{k} vector and the magnetization. Details on the sample preparation can be found in earlier works.^{53,54}

IV. RESULTS AND DISCUSSION

A. Shape of spectral peaks

$L_{2,3}$ edge XANES and XMCD spectra calculated using the plain LSDA and using the LSDA+DMFT with the AMF d.c. correction are shown in Fig. 1, together with our experimental data. These experimental spectra are similar to spectra measured earlier for Fe and Co (see Ref. 55) and for Ni (see Ref. 56). One can see that inclusion of the correlations in the d band changes the peak intensities as well as the shapes of the main peaks. In particular, a more pronounced asymmetry of the L_3 peak appears in the LSDA+DMFT spectra, leading to a better agreement with experiment. The changes are, nevertheless, not very big (they are more visible

in Fig. 2 below). This may appear surprising given the fact that for photoemission spectra of these systems, the inclusion of dynamic correlations via the LSDA+DMFT has a very pronounced effect as compared to the LSDA.¹⁵ However, the self-energy $\hat{\Sigma}(E)$ is relatively small in the regime of unoccupied states³⁸ so it is actually plausible that its effect on the XAS is not very pronounced.

As it was mentioned in the introduction, in order to remedy many deficiencies of the LSDA as concerns the ground-state properties such as μ_{orb} , it is sufficient to include the correlations in a static way only via the OP Brooks scheme or via the LSDA+ U . However, these schemes do not bring any significant improvement concerning XAS. We demonstrate this by showing in Fig. 2 spectra calculated via the LSDA and via the LSDA+ U (the dashed and dash-dotted lines). We used the same U and J parameters for the LSDA+ U calculations as for the LSDA+DMFT calculations. Spectra obtained via the OP Brooks scheme are practically indistinguishable from the LSDA+ U results, so they are not shown here. Fig. 2 shows that the LSDA+ U method does not significantly alter the calculated spectra of transition metals with respect to the LSDA, similarly as it was found earlier for the OP Brooks scheme.⁵⁷ This is in line with the concept that the OP Brooks scheme can be seen in fact as one of the limits of the more general LSDA+ U concept.¹³

It was mentioned earlier in Sec. II that there are several ways to correct for the d.c. error in the LSDA+DMFT. Even though the AMF scheme seems to be the most reasonable d.c. procedure for $3d$ TMs, one cannot *a priori* exclude the possibility that another d.c. scheme might be more appropriate for XAS. Therefore we checked how the results change if the AAL d.c. scheme is employed instead of the AMF scheme. We found that the calculated spectra look quite similar (Fig. 2, dotted lines and full lines). A closer inspection of

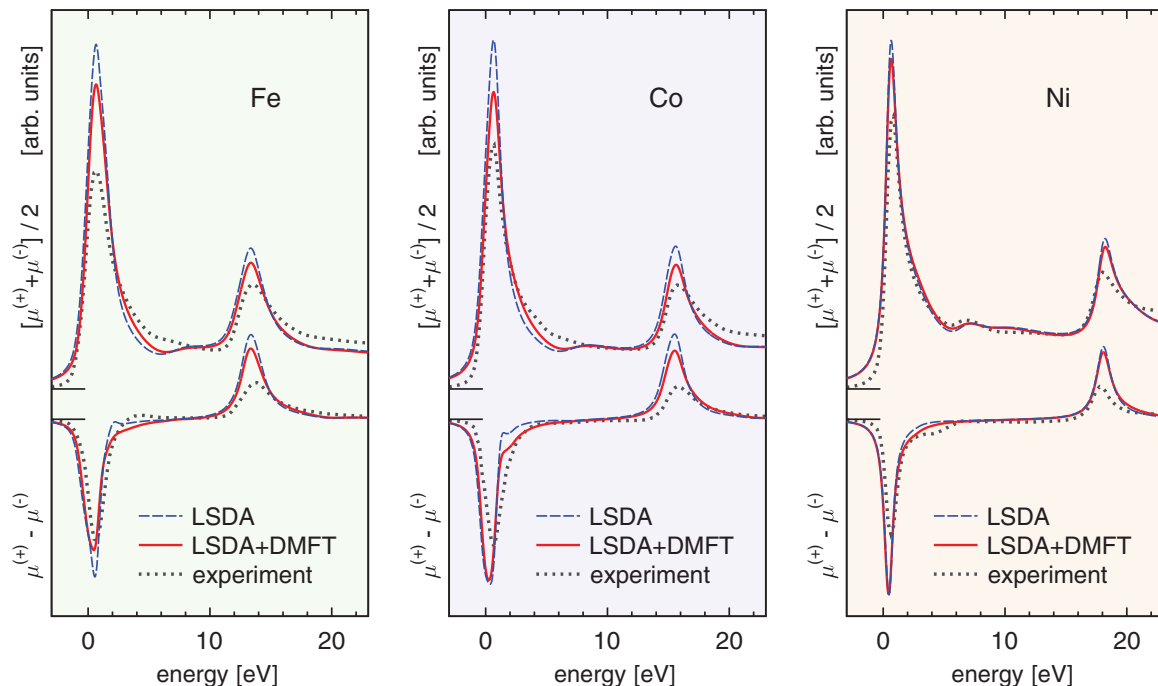


FIG. 1. (Color online) $L_{2,3}$ edge XANES and XMCD spectra of Fe, Co, and Ni calculated on the basis of the plain LSDA and of the LSDA+DMFT with the AMF d.c. correction, compared to experiment.

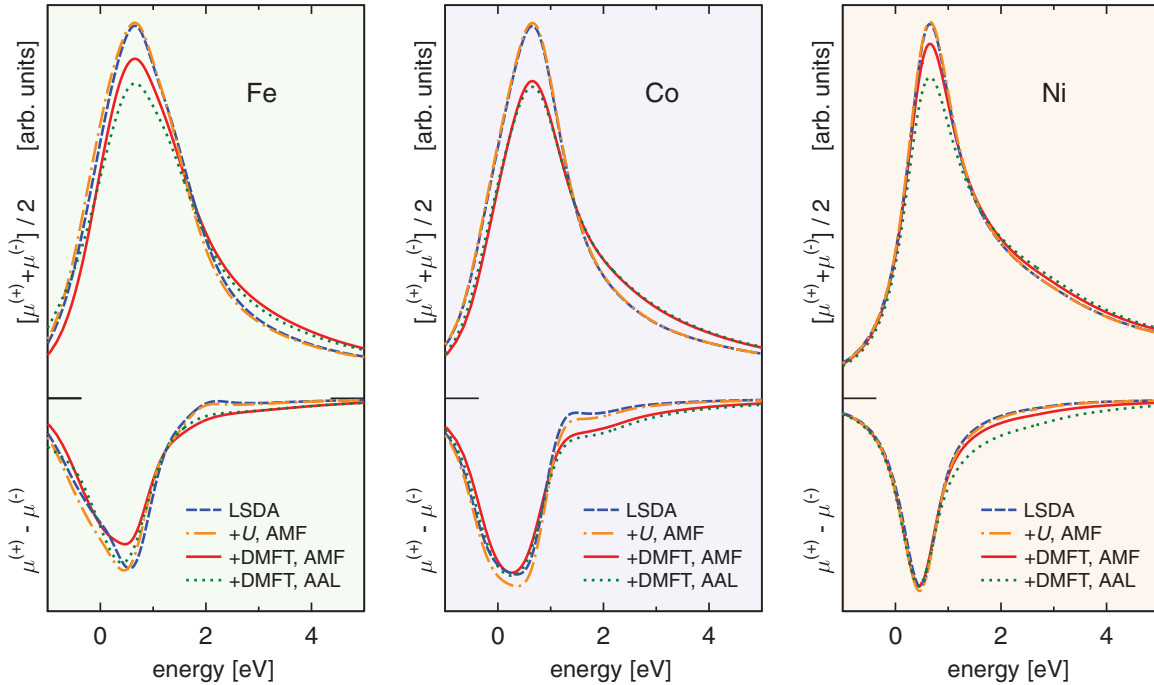


FIG. 2. (Color online) L_3 edge XANES and XMCD spectra for Fe, Co, and Ni calculated via the plain LSDA, via the LSDA+ U with the AMF d.c. correction, via the LSDA+DMFT with the AMF d.c. correction, and via the LSDA+DMFT with the AAL d.c. correction.

Fig. 2 reveals further that the calculated spectra split into two groups, according to whether the dynamic effects to the self-energy have been included (LSDA+DMFT calculations) or not (LSDA and LSDA+ U calculations). This is especially evident for the XANES spectra; e.g., in the case of Co, only two spectral curves can in fact be distinguished because the results are pairwise practically identical (upper part of the middle panel in Fig. 2). For the XMCD spectra, this splitting of the four spectra into two groups is clearly visible at the high-energy end of the Fe and Co L_3 peaks between 1–3 eV in Fig. 2. The choice of the d.c. model has thus only a minor influence on the shapes of XANES and XMCD spectra. Nevertheless, it has some influence on the intensities of the peaks (see the following section).

Thanks to the smaller energy range of Fig. 2, the changes in the asymmetry of the L_3 white line are more apparent in this figure than in Fig. 1. In particular, one can see that the XAS curves for the plain LSDA and for the LSDA+DMFT intersect at about 1.5 eV. For Ni, the LSDA and LSDA+DMFT results are very similar, nevertheless, the intersection of the curves still can be distinguished.

B. Relation to magnetic moments

X-ray absorption spectroscopy has been very helpful in studying magnetism. Magnetism is also a domain where correlations between the d electrons may be quite important. Generally, if correlations are included via the DMFT, the spin magnetic moment μ_{spin} of $3d$ TMs changes only slightly while the orbital magnetic moment μ_{orb} significantly increases relative to the values obtained for the LSDA.¹⁸ This is also illustrated by our results summarized in Table I. We show results for the FLEX solver here, the results for the TMA

solver differ by 3% at most. A detailed investigation of the influence of the model parameters on magnetic moments has been done by Chadov *et al.*¹⁸

It may come surprising that while the inclusion of d band correlations leads to significant changes in the ground-state properties as reflected by μ_{orb} , the changes in the XANES and XMCD spectra are not so apparent (see Fig. 1). Indeed, one may ask to what degree are the changes significant at all: do they really reflect the different treatment of the correlations? Let us assess the significance of the changes in the spectra by comparing them with the changes of an appropriate ground-state property. A suitable quantity in this respect is the $\mu_{\text{orb}}/\mu_{\text{spin}}$ ratio, because it is underestimated by the plain LSDA while it is correctly described by the LSDA+DMFT method. By applying the XMCD sum rules (5)–(6) to the theoretical spectrum, the ratio between the d components of the magnetic moments, $\mu_{\text{orb}}^{(d)}/\mu_{\text{spin}}^{(d)}$, can be obtained and compared to the $\mu_{\text{orb}}^{(d)}/\mu_{\text{spin}}^{(d)}$ ratio obtained directly from the ground-state electronic structure. If this is done for different ways of accounting for the many-body effects, the consistency of the changes in the spectra and in the ground-state properties can be monitored.

TABLE I. Magnetic moments (in units of μ_B) for Fe, Co, and Ni calculated via the plain LSDA and via the LSDA+DMFT with the AMF d.c. correction.

	Fe	Co	Ni
μ_{spin} (LSDA)	2.26	1.60	0.63
μ_{spin} (LSDA+DMFT)	2.18	1.65	0.68
μ_{orb} (LSDA)	0.052	0.079	0.051
μ_{orb} (LSDA+DMFT)	0.094	0.155	0.071

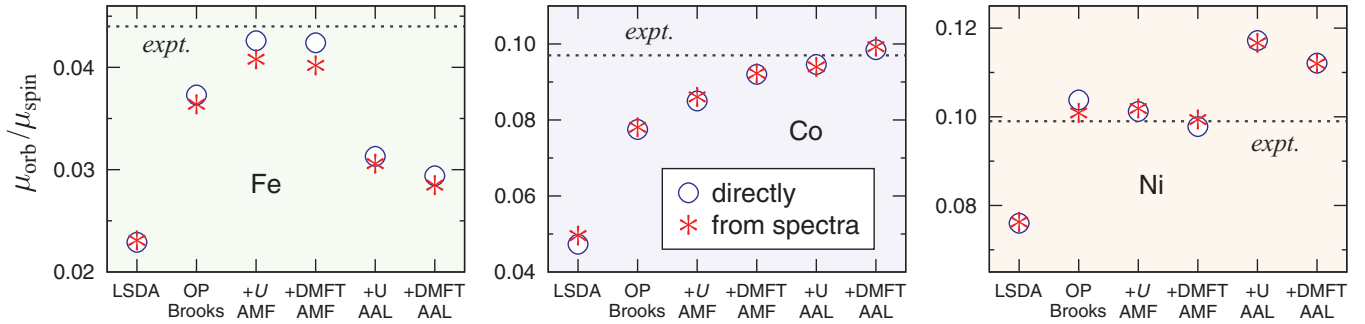


FIG. 3. (Color online) The $\mu_{\text{orb}}^{(d)}/\mu_{\text{spin}}^{(d)}$ ratio evaluated directly and from theoretical XMCD spectra for calculations employing plain LSDA, OP Brooks, LSDA+ U with the AMF d.c. correction (denoted as “+ U AMF” on the horizontal axis), LSDA+DMFT with the AMF d.c. correction (“+DMFT AMF”), LSDA+ U with the AAL d.c. correction (“+ U AAL”), and LSDA+DMFT with the AAL d.c. correction (“+DMFT AAL”). The experimental ratios were taken those obtained from magnetomechanical measurements.⁵⁸

Our results are summarized in Fig. 3, where the $\mu_{\text{orb}}^{(d)}/\mu_{\text{spin}}^{(d)}$ ratio evaluated by the two ways mentioned above is shown for the plain LSDA, the OP Brooks scheme, the LSDA+ U and the LSDA+DMFT with the AMF d.c. correction, and the LSDA+ U and the LSDA+DMFT with the AAL d.c. correction. The $\mu_{\text{orb}}/\mu_{\text{spin}}$ ratio derived from magnetomechanical experiments is shown for comparison.⁵⁸ Use of $\mu_{\text{orb}}/\mu_{\text{spin}}$ instead of $\mu_{\text{orb}}^{(d)}/\mu_{\text{spin}}^{(d)}$ as an experimental reference is justified because both ratios differ by less than 5% and our focus is not on the agreement of μ_{orb} with experiment (μ_{orb} depends also on the value of U anyway).¹⁸

It is obvious that the changes of the intensities of the L_3 and L_2 XMCD peaks reflect changes in $\mu_{\text{orb}}/\mu_{\text{spin}}$ via the sum rules very accurately. The differences between spectra calculated by different ways of dealing with the many-body effects are therefore relevant and plausible. Even relatively small changes in the intensities of XMCD peaks in Fig. 1 correspond to large changes in μ_{orb} , as can be seen in Table I. The influence of the correlations between the d electrons on the occupied states (as reflected by the magnetic moments) and on the unoccupied states (as reflected by the x-ray spectra) is thus described consistently.

It follows from our analysis that the failure of the LSDA to reproduce the ratio of the L_3/L_2 XMCD peak intensities cannot be a simple consequence of the failure of the LSDA to yield correct orbital moments μ_{orb} .

C. Effect of the core hole within the final-state approximation

Accounting for the correlations in the d band via the LSDA+DMFT improves the calculated spectra but the improvement is not dramatic (Fig. 1). A better agreement with experiment could presumably be obtained if the core hole was accounted for. This is quite a complicated task within the *ab initio* scheme. A technically relatively simple way of achieving this is via the “static” final-state approximation (see Sec. II). For the K edges, such a scheme sometimes improves the XANES (e.g., for the Zn edge in ZnSe⁵⁹ or for the Si edge in quartz)⁶⁰ while sometimes it has only a minor effect (early transition metals).⁴⁵ However, the final-state approximation need not work for the $L_{2,3}$ edges, which involve transitions to semilocalized d states; by promoting a $2p$ electron into the valence states one may effectively fill the d band of

the photoabsorbing atom, suppressing to a large extent the intensity of the white line. This issue will be explored in the following.

To see the effect of the final-state approximation, we applied it on top of the LSDA+DMFT procedure. The results are shown in Fig. 4. It is evident that this procedure does not generally improve the $L_{2,3}$ edge spectra of late 3d TMs. Hardly any systematic trend in the effect of the core hole can be found neither as concerns the shape of the white lines nor as concerns the ratio of the intensities of the L_3 and L_2 peaks. For Fe, we observe an increase of the ratio of intensities of the L_3 and L_2 XMCD peaks, in agreement with experiment. For Co, the final-state approximation produces only minor changes with respect to the ground-state calculations. For Ni, however, including the core hole via the final-state approximation substantially worsens the agreement with experiment—the XAS white lines as well as the prominent XMCD peaks practically disappear! A similar situation occurs if the final-state approximation is applied over the plain LSDA (therefore only the LSDA+DMFT results are shown here).

Application of the final-state rule for Ni has a much more dramatic effect than for Fe or Co. Intuitively, this can be understood by considering the number of holes in the d band. For the ground state, our calculation yields the following numbers of the holes $n_h^{(d)}$: 3.48 (Fe), 2.48 (Co), and 1.45 (Ni). These numbers are practically the same for the LSDA and for the LSDA+DMFT. If the final-state rule is applied, $n_h^{(d)}$ at the photoabsorbing atom decreases to 2.36 (Fe), 1.36 (Co), and 0.46 (Ni). So in the atomic-like picture, there are very few holes left in the d band for Ni and the white line is thus strongly suppressed. Also the relative decrease of $n_h^{(d)}$ is larger for Ni (by 68%) than for Fe (by 32%) or Co (by 45%), which is again consistent with the changes in the white line intensities in Fig. 4. This is, of course, only an intuitive view that cannot be taken too literally. In any case, if the final-state rule dramatically fails for Ni, it cannot be trusted to produce reliable results for Fe or Co either.

We tested the final-state rule also with a half-filled core hole, which can be seen as employing the Slater transition-state method. Sometimes this procedure works well for the K edge spectra.^{61,62} Satisfying results were also reported for the Cu L_3 edge XANES.⁶³ In our case, however, the Slater transition-state method does not bring any substantial improvement; the

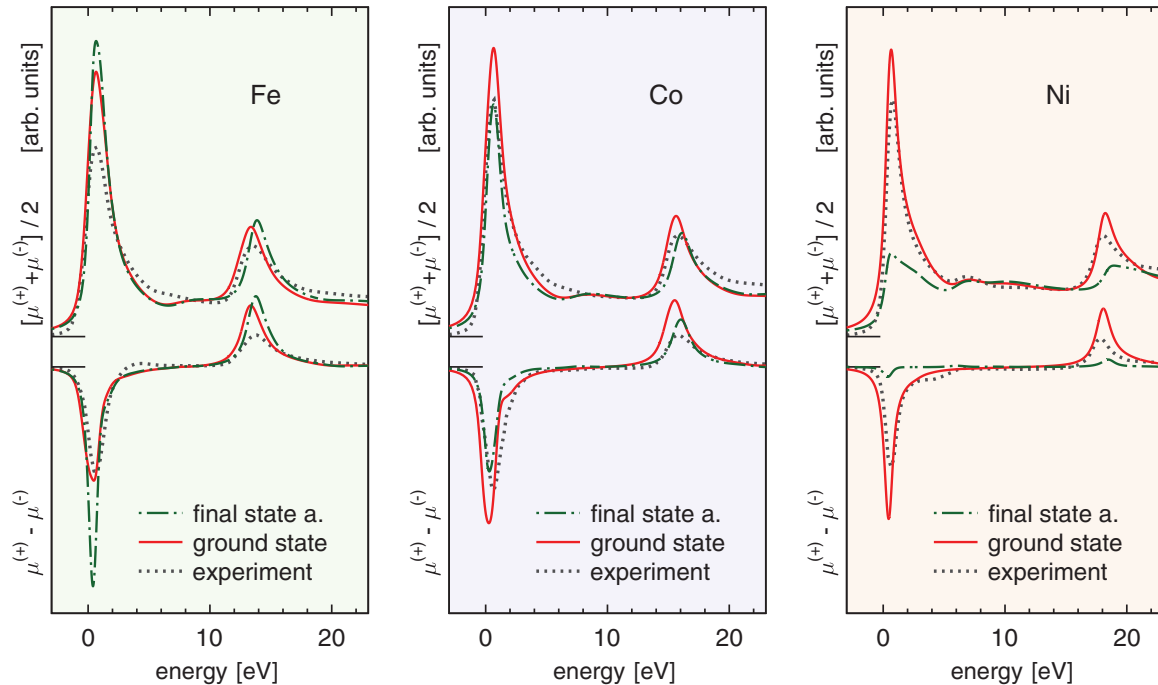


FIG. 4. (Color online) $L_{2,3}$ edge XANES and XMCD spectra of Fe, Co, and Ni calculated within the LSDA+DMFT when the core hole is ignored (using the ground-state potential) and when the core hole is included via the final-state approximation. Experimental XANES and XMCD spectra are shown for comparison.

results just lie approximately half-way between the results obtained without a core hole and with a full core hole, so we do not show them.

Our results can be compared with earlier results based on various versions of the Hubbard Hamiltonian where the interaction between the core hole and the photoelectron was taken into account beyond the mean-field level. Calculations of the Ni $L_{2,3}$ edge XAS and XMCD based on the Anderson impurity model, with the ground state described as a superposition of d^{10} , d^9 , and d^8 configurations and including the interaction between electrons, which produce atomic multiplets, led to quite a symmetric XAS lineshape.^{64,65} This symmetry may be an artifact of the essentially atomic-like model employed in the calculations, because our band-structure-based approach produces an asymmetric L_3 XAS white line for Ni in the plain LSDA as well as in the LSDA+DMFT mode (Fig. 1). For the Ni L_2 edge, the asymmetry of the white line is not so well reproduced by our LSDA or LSDA+DMFT calculations and the same is even more true for the Anderson impurity model.^{64,65}

A lot of attention was devoted to the “satellites,” which appear in the experimental Ni $L_{2,3}$ edge spectra at 6–7 eV for XAS and at 4 eV in the XMCD (see Fig. 1). The Anderson impurity model calculations reproduce these peaks at the same energy for XAS and XMCD, at about 4 eV.^{64,65} Our calculations reproduce the XAS satellite peak at about 7 eV but not the XMCD satellite peak; there is practically no difference between the plain LSDA and the LSDA+DMFT calculations or between the ground-state and the final-state-rule calculations in this respect. It thus appears that the peak, which is found at 6–7 eV in the experimental XAS, comes from the long-range order, which is included in our calculation but

is absent in the Anderson impurity model calculations. On the other hand, the peak, that is found at 4 eV in the experimental Ni L_3 edge XMCD is probably connected with the core-hole interaction, which the ground-state calculation ignores and the final-state-rule calculations includes only incompletely. The XAS counterpart^{64,65} of this XMCD peak is then hidden in the high-energy shoulder of the Ni L_3 white line; this shoulder seems to miss in the Anderson impurity model calculation.

About the same time when this manuscript was submitted, Pardini *et al.*⁶⁶ published calculations of $L_{2,3}$ edge XAS and XMCD of Fe, Co, and Ni based on a generalized Hubbard Hamiltonian. In their approach, the interaction between the valence d electrons and the core p electrons as well as the interaction between the valence d electrons themselves is included explicitly in the Hamiltonian (via parametrized terms). The band-structure effects enter the calculations via orbital coefficients obtained from *ab initio* calculations.⁶⁶ Unlike our approach, this scheme is not self-consistent, i.e., the charge density is the same as in the LSDA. The spectra obtained using this approach show a distinct asymmetry of the XAS white lines,⁶⁶ similarly to our results. The asymmetry of the peaks for Fe and Co is larger in the calculations of Pardini *et al.* than in our calculations. This is probably due to the core hole interaction, which is explicitly included in the work of Pardini *et al.*⁶⁶ For Ni, the calculations based on the generalized Hubbard Hamiltonian yield results similar to single-particle calculations,⁶⁶ which is again similar to what we observe concerning the differences between spectra obtained using the plain LSDA and using the LSDA+DMFT (see Fig. 1). Interestingly, the asymmetry of the XMCD spectra obtained by the generalized Hubbard Hamiltonian calculations of Pardini *et al.*⁶⁶ is too large and the relative intensities of

the L_3 and L_2 XMCD peaks remain the same as in their single-particle calculations without the core hole. Pardini *et al.*⁶⁶ give no data on the magnetic moments so it is not possible to assess how suitable their scheme is for describing spin and orbital magnetism.

As a whole, our results demonstrate that the final-state approximation is unsuitable for describing the $L_{2,3}$ edge XAS and XMCD in late $3d$ TMs. This applies for calculations based on the plain LSDA as well as on the LSDA+DMFT method. The work of Pardini *et al.* shows that including the core-hole interaction as an additional term in the generalized Hubbard Hamiltonian seems to improve the XAS spectra but fails to reproduce the XMCD peaks intensities.⁶⁶ It appears that another approach is needed to deal with the core hole, valence-band correlations, and band-structure effects simultaneously to yield more accurate $L_{2,3}$ edge XMCD spectra of TMs. A possible way could be to apply the linear-response time-dependent density-functional formalism^{2,3} on top of the LSDA+DMFT scheme.

V. CONCLUSIONS

Our goal was to find out whether the differences commonly occurring between the experimental $L_{2,3}$ edge XANES and XMCD spectra of $3d$ transition metals on the one hand and *ab initio* calculations on the other hand are mainly due to the way the LSDA deals with the correlations. By performing

the LSDA+DMFT calculations, we found that if valence- and conduction-band correlations are included, the spectra change in the right direction with respect to the plain LSDA. In particular, the LSDA+DMFT yields asymmetric L_3 XAS white lines. The improvement is, however, rather incremental than dramatic. The ratio of the intensities of the L_3 and L_2 XAS and XMCD peaks is not significantly improved by the LSDA+DMFT formalism. The changes in the intensities of the XMCD peaks are, nevertheless, consistent with the changes of the $\mu_{\text{orb}}/\mu_{\text{spin}}$ ratio as suggested by the XMCD sum rules.

When the core hole is additionally accounted for within the final-state approximation, the agreement between theory and experiment generally does not improve (in the case of Ni, it substantially worsens). It appears, therefore, that to get a decisive improvement of *ab initio* calculations of the $L_{2,3}$ edge XAS and XMCD spectra of $3d$ metals, the dynamic correlations between the excited photoelectron and the core hole have to be taken into account.

ACKNOWLEDGMENTS

This work was supported by the Grant Agency of the Czech Republic within the project 108/11/0853, by the Deutsche Forschungsgemeinschaft through FOR 1346 and by the German ministry BMBF under Contract 05KS10WMA. The research in the Institute of Physics AS CR was supported by the Academy of Sciences of the Czech Republic.

*sipr@fzu.cz; <http://www.fzu.cz/~sipr>

†hubert.ebert@cup.uni-muenchen.de;

<http://ebert.cup.uni-muenchen.de>.

¹H. Wende, *Rep. Prog. Phys.* **67**, 2105 (2004).

²J. Schwitalla and H. Ebert, *Phys. Rev. Lett.* **80**, 4586 (1998).

³A. L. Ankudinov, A. I. Nesvizhskii, and J. J. Rehr, *Phys. Rev. B* **67**, 115120 (2003).

⁴M. Alouani, J. M. Wills, and J. W. Wilkins, *Phys. Rev. B* **57**, 9502 (1998).

⁵O. Šipr and H. Ebert, *Phys. Rev. B* **72**, 134406 (2005).

⁶P. Carra, B. T. Thole, M. Altarelli, and X. Wang, *Phys. Rev. Lett.* **70**, 694 (1993).

⁷B. T. Thole, P. Carra, F. Sette, and G. van der Laan, *Phys. Rev. Lett.* **68**, 1943 (1992).

⁸A. Scherz, H. Wende, K. Baberschke, J. Minár, D. Benea, and H. Ebert, *Phys. Rev. B* **66**, 184401 (2002).

⁹K. Baberschke, *Phys. Scr.*, **T 115**, 49 (2005).

¹⁰H. Wende, A. Scherz, C. Sorg, K. Baberschke, E. K. U. Gross, H. Appel, K. Burke, J. Minár, H. Ebert, A. L. Ankudinov, and J. J. Rehr, *AIP Conf. Proc.* **882**, 78 (2007).

¹¹O. Eriksson, B. Johansson, R. C. Albers, A. M. Boring, and M. S. S. Brooks, *Phys. Rev. B* **42**, 2707 (1990).

¹²I. V. Solovyev, *Phys. Rev. Lett.* **95**, 267205 (2005).

¹³I. V. Solovyev, A. I. Liechtenstein, and K. Terakura, *Phys. Rev. Lett.* **80**, 5758 (1998).

¹⁴J. Minár, H. Ebert, C. De Nadaï, N. B. Brookes, F. Venturini, G. Ghiringhelli, L. Chioncel, M. I. Katsnelson, and A. I. Liechtenstein, *Phys. Rev. Lett.* **95**, 166401 (2005).

¹⁵J. Braun, J. Minár, H. Ebert, M. I. Katsnelson, and A. I. Liechtenstein, *Phys. Rev. Lett.* **97**, 227601 (2006).

¹⁶J. Sánchez-Barriga, J. Fink, V. Boni, I. Di Marco, J. Braun, J. Minár, A. Varykhalov, O. Rader, V. Bellini, F. Manghi, H. Ebert, M. I. Katsnelson, A. I. Liechtenstein, O. Eriksson, W. Eberhardt, and H. A. Dürr, *Phys. Rev. Lett.* **103**, 267203 (2009).

¹⁷J. Sánchez-Barriga, J. Minár, J. Braun, A. Varykhalov, V. Boni, I. Di Marco, O. Rader, V. Bellini, F. Manghi, H. Ebert, M. I. Katsnelson, A. I. Liechtenstein, O. Eriksson, W. Eberhardt, H. A. Dürr, and J. Fink, *Phys. Rev. B* **82**, 104414 (2010).

¹⁸S. Chadov, J. Minár, M. I. Katsnelson, H. Ebert, D. Ködderitzsch, and A. I. Liechtenstein, *Europhys. Lett.* **82**, 37001 (2008).

¹⁹O. Šipr, J. Minár, S. Mankovsky, and H. Ebert, *Phys. Rev. B* **78**, 144403 (2008).

²⁰F. de Groot and A. Kotani, *Core level spectroscopy of solids*, Advances in Condensed Matter Science 6 (CRC Press, Boca Raton, 2008).

²¹H. Ikeno, F. M. F. de Groot, E. Stavitski, and I. Tanaka, *J. Phys. Condens. Matter* **21**, 104208 (2009).

²²C. R. Natoli, M. Benfatto, C. Brouder, M. F. Ruiz Lopez, and D. L. Foulis, *Phys. Rev. B* **42**, 1944 (1990).

²³P. Krüger, *Phys. Rev. B* **81**, 125121 (2010).

²⁴E. L. Shirley, *Phys. Rev. Lett.* **80**, 794 (1998).

²⁵R. Laskowski and P. Blaha, *Phys. Rev. B* **82**, 205104 (2010).

²⁶J. Minár, L. Chioncel, A. Perlov, H. Ebert, M. I. Katsnelson, and A. I. Liechtenstein, *Phys. Rev. B* **72**, 045125 (2005).

²⁷J. Minár, *J. Phys. Condens. Matter* **23**, 253201 (2011).

- ²⁸G. Kotliar, S. Y. Savrasov, K. Haule, V. S. Oudovenko, O. Parcollet, and C. A. Marianetti, *Rev. Mod. Phys.* **78**, 865 (2006).
- ²⁹K. Held, *Adv. Phys.* **56**, 829 (2007).
- ³⁰H. Ebert, in *Electronic Structure and Physical Properties of Solids*, Lecture Notes in Physics Vol. 535, edited by H. Dreyssé (Springer, Berlin, 2000), p. 191.
- ³¹S. H. Vosko, L. Wilk, and M. Nusair, *Can. J. Phys.* **58**, 1200 (1980).
- ³²T. Huhne, C. Zecha, H. Ebert, P. H. Dederichs, and R. Zeller, *Phys. Rev. B* **58**, 10236 (1998).
- ³³T. Huhne and H. Ebert, *Solid State Commun.* **109**, 577 (1999).
- ³⁴L. V. Pourovskii, M. I. Katsnelson, and A. I. Lichtenstein, *Phys. Rev. B* **72**, 115106 (2005).
- ³⁵S. Chadov, Ph.D. thesis, Universität München, 2007.
- ³⁶V. I. Anisimov and O. Gunnarsson, *Phys. Rev. B* **43**, 7570 (1991).
- ³⁷I. Yang, S. Y. Savrasov, and G. Kotliar, *Phys. Rev. Lett.* **87**, 216405 (2001).
- ³⁸A. Grechnev, I. Di Marco, M. I. Katsnelson, A. I. Lichtenstein, J. Wills, and O. Eriksson, *Phys. Rev. B* **76**, 035107 (2007).
- ³⁹O. Miura and T. Fujiwara, *Phys. Rev. B* **77**, 195124 (2008).
- ⁴⁰H. J. Vidberg and J. W. Serene, *J. Low Temp. Phys.* **29**, 179 (1977).
- ⁴¹A. G. Petukhov, I. I. Mazin, L. Chioncel, and A. I. Lichtenstein, *Phys. Rev. B* **67**, 153106 (2003).
- ⁴²E. R. Ylvisaker, W. E. Pickett, and K. Koepf, *Phys. Rev. B* **79**, 035103 (2009).
- ⁴³M. T. Czyzyk and G. A. Sawatzky, *Phys. Rev. B* **49**, 14211 (1994).
- ⁴⁴P. J. Braspenning, R. Zeller, A. Lodder, and P. H. Dederichs, *Phys. Rev. B* **29**, 703 (1984).
- ⁴⁵R. Zeller, *Z. Phys. B* **72**, 79 (1988).
- ⁴⁶K. Jorissen and J. J. Rehr, *Phys. Rev. B* **81**, 245124 (2010).
- ⁴⁷F. A. Shamma, M. Abbate, and J. C. Fuggle, in *Unoccupied Electron States*, edited by J. C. Fuggle and J. E. Inglesfield (Springer Verlag, Berlin, 1992), p. 347.
- ⁴⁸J. L. Campbell and T. Papp, *At. Data Nucl. Data Tables* **7**, 1 (2001).
- ⁴⁹J. E. Müller, O. Jepsen, and J. W. Wilkins, *Solid State Commun.* **42**, 365 (1982).
- ⁵⁰M. Benfatto, S. Della Longa, and C. R. Natoli, *J. Synchrotron Radiat.* **10**, 51 (2003).
- ⁵¹J. Stöhr, *J. Magn. Magn. Mater.* **200**, 470 (1999).
- ⁵²O. Šipr, J. Minár, and H. Ebert, *Europhys. Lett.* **87**, 67007 (2009).
- ⁵³A. Scherz, H. Wende, and K. Baberschke, *Appl. Phys. A* **78**, 843 (2004).
- ⁵⁴A. Scherz, Ph.D. thesis, Freie Universität Berlin, 2004.
- ⁵⁵C. T. Chen, Y. U. Idzerda, H. J. Lin, N. V. Smith, G. Meigs, E. Chaban, G. H. Ho, E. Pellegrin, and F. Sette, *Phys. Rev. Lett.* **75**, 152 (1995).
- ⁵⁶C. T. Chen, F. Sette, Y. Ma, and S. Modesti, *Phys. Rev. B* **42**, 7262 (1990).
- ⁵⁷H. Ebert, *Solid State Commun.* **100**, 677 (1996).
- ⁵⁸R. A. Reck and D. L. Fry, *Phys. Rev.* **184**, 492 (1969).
- ⁵⁹O. Šipr, P. Machek, A. Šimůnek, J. Vackář, and J. Horák, *Phys. Rev. B* **56**, 13151 (1997).
- ⁶⁰Z. Y. Wu, F. Jollet, and F. Seifert, *J. Phys. Condens. Matter* **10**, 8083 (1998).
- ⁶¹T. Mizoguchi, I. Tanaka, M. Yoshiya, F. Oba, K. Ogasawara, and H. Adachi, *Phys. Rev. B* **61**, 2180 (2000).
- ⁶²M. Leetmaa, M. P. Ljungberg, A. Lyubartsev, A. Nilsson, and L. G. M. Pettersson, *J. Electron Spectrosc. Relat. Phenom.* **177**, 135 (2010).
- ⁶³J. Luitz, M. Maier, C. Hébert, P. Schattschneider, P. Blaha, K. Schwarz, and B. Jouffrey, *Eur. Phys. J. B* **21**, 363 (2001).
- ⁶⁴T. Jo and G. A. Sawatzky, *Phys. Rev. B* **43**, 8771 (1991).
- ⁶⁵G. van der Laan and B. T. Thole, *J. Phys. Condens. Matter* **4**, 4181 (1992).
- ⁶⁶V. B. L. Pardini and F. Manghi, *J. Phys. Condens. Matter* **23**, 215601 (2011).